ADVANCED FUNCTIONAL MATERIALS
www.afm-journal.de

www.MaterialsViews.com

Near-Infrared Emitting and Pro-Angiogenic Electrospun Conjugated Polymer Scaffold for Optical Biomaterial Tracking

*Abeni Wickham, Daniel Sjölander, Gunnar Bergström, Ergang Wang, Vijayalakshmi Rajendran, Camilla Hildesjö, Karin Skoglund, K. Peter R. Nilsson, and Daniel Aili**

Noninvasive tracking of biomaterials is vital for determining the fate and degradation of an implant in vivo, and to show its role in tissue regeneration. Current biomaterials have no inherent capacity to enable tracing but require labeling with, for example, fluorescent dyes, or nanoparticles. Here a novel biocompatible fully conjugated electrospun scaffold is described, based on a semiconducting luminescent polymer that can be visualized in situ after implantation using fluorescence imaging. The polymer, poly [2,3-bis-(3-octyloxyphenyl)quinoxaline-5,8-diyl-*alt*-thiophene-2,5-diyl] (TQ1), is electrospun to form a fibrous mat. The fibers display fluorescence emission in the near-infrared region with lifetimes in the sub-nanosecond range, optimal for in situ imaging. The material shows no cytotoxic behaviors for embryonic chicken cardiomyocytes and mouse myoblasts, and cells migrate onto the TQ1 fibers even in the presence of a collagen substrate. Subcutaneous implantations of the material in rats show incorporation of the TQ1 fibers within the tissue, with limited inflammation and a preponderance of small capillaries around the fibers. The fluorescent properties of the TQ1 fibers are fully retained for up to 90 d following implantation and they can be clearly visualized in tissue using fluorescence and lifetime imaging, thus making it both a pro-angiogenic and traceable biomaterial.

1. Introduction

Biomaterial strategies for regenerating tissue offer solutions to people with ailing body parts, without the need for donor tissue. Significant progress has been made in the development of polymeric scaffolds for tissue engineering and cell-based therapies, primarily focusing on improving biocompatibility, and the material's mechanical and structural properties.[1,2] Recent efforts have been devoted to increasing the biofunctionality of biomaterials by incorporating instructive signals for the modulation of attachment, proliferation, and differentiation of cells.[3–5] A variety of approaches have also been reported to provide scaffold materials with pro-angiogenic properties, since vascularization is crucial for the successful integration of the tissue-engineered construct, as it allows for the adequate exchange of oxygen and nutrients required for cell survival and consequently, tissue regeneration.[6,7]

A. Wickham, Prof. D. Aili
Division of Molecular Physics
Department of Physics
Chemistry and Biology (IFM)
Linköping University
SE-581 83 Linköping, Sweden
E-mail: daniel.aili@liu.se

Dr. D. Sjölander, Prof. K. P. R. Nilsson
Division of Organic Chemistry
Department of Physics
Chemistry and Biology (IFM)
Linköping University
SE-581 83 Linköping, Sweden

G. Bergström
Division of Biotechnology
Department of Physics
Chemistry and Biology (IFM)
Linköping University
SE-581 83 Linköping, Sweden

Dr. E. Wang
Department of Chemistry
and Chemical Engineering/Polymer Technology
Chalmers University of Technology
SE-412 96 Göteborg, Sweden

V. Rajendran[+]
Integrative Regenerative Medicine (IGEN) Centre
and Department of Clinical and Experimental Medicine
Linköping University
SE-581 83 Linköping, Sweden

C. Hildesjö, Dr. K. Skoglund
Department of Clinical Pathology
Council of Östergötland
Linköping University Hospital
SE-581 91 Linköping, Sweden

[+]Present address: Section of Immunity, Infection and Inflammation (Ocular Immunology), Division of Applied Medicine, School of Medicine and Dentistry, Institute of Medical Sciences, Foresterhill, University of Aberdeen, Aberdeen, AB25 2ZD Scotland, UK

DOI: 10.1002/adfm.201500351

In order to verify the in vivo response of an implant, and to facilitate translation of new materials into clinical applications, it is critical to be able to accurately determine the fate and efficacy of the implant.[8,9] Traditional noninvasive imaging techniques, such as magnetic resonance imaging (MRI) and computed tomography (CT), are typically used to track an implant and to monitor its effect on tissue regeneration.[10,11] While implants made from, e.g., titanium, cobalt–chromium alloys, and ceramics, are easily discriminated from the tissue, soft biomacromolecular or polymer-based materials are very difficult to image and often require resecting the tissue to assess the fate of the implant.[12] Numerous strategies have thus been proposed to facilitate noninvasive tracing of polymeric implants using either ultrasound, MRI, X-ray, or fluorescent imaging, but these required extensive modifications to an already optimized material with, e.g., fluorescent protein tags, nanoparticles, single walled carbon nanotube fluorophores, and light sensitive degradable polymers.[13–16] A biomaterial that is inherently traceable, while providing the scaffolding support needed for tissue regeneration, would thus be highly attractive.

High molecular weight conjugated polymers (CPs) are a class of macromolecules that can fulfill these criteria. Conductive CPs have been used in a wide range of biomaterials applications, including heart and neural regeneration,[17] and can be processed into micrometer and sub-micrometer sized fibers using electrospinning.[18] For tissue engineering applications CPs are typically combined with more biocompatible polymers, either as coatings or as blends.[19] CPs can also demonstrate highly interesting fluorescence and molecular recognition properties, which have been used for in vivo amyloid diagnostics,[20] tracking and imaging of drug releasing polymer nanoparticles,[21] and sensing applications.[22]

In this work we have developed a highly biocompatible fibrous biomaterial scaffold using a conjugated luminescent polymer that enables convenient tracing of the material in tissue without the need for further modifications. The polymer, poly[2,3-bis-(3-octyloxyphenyl)quinoxaline- 5,8-diyl-*alt*-thiophene-2,5-diyl] (TQ1) (**Figure 1**a) is based on thiophene and quinoxaline and was originally developed as a low bandgap polymer for organic solar cell applications.[23] Electrospinning of TQ1 yields a fibrous material that can be visualized in tissue using noninvasive fluorescence imaging and also demonstrates excellent biocompatibility, tissue integration, and stimulates formation of blood vessels within the implant. The TQ1 fibers emit in the near infrared region (NIR), which makes it possible to characterize the material in vivo. In this wavelength range, techniques such as two-photon microscopy and in vivo fluorescence confocal imaging can image materials in the millimeter depth range in tissue.[24,25] The difference in fluorescence and lifetimes between the surrounding tissue and the TQ1 fiber is stark and the TQ1 can thus be easily distinguished from tissue autofluorescence during integration and regeneration. Additionally, this material can be combined with other commonly used biomaterials, such as collagen hydrogels, to both improve their functionality and biocompatibility to obtain implants that promote tissue regeneration that can be monitored using noninvasive imaging techniques.

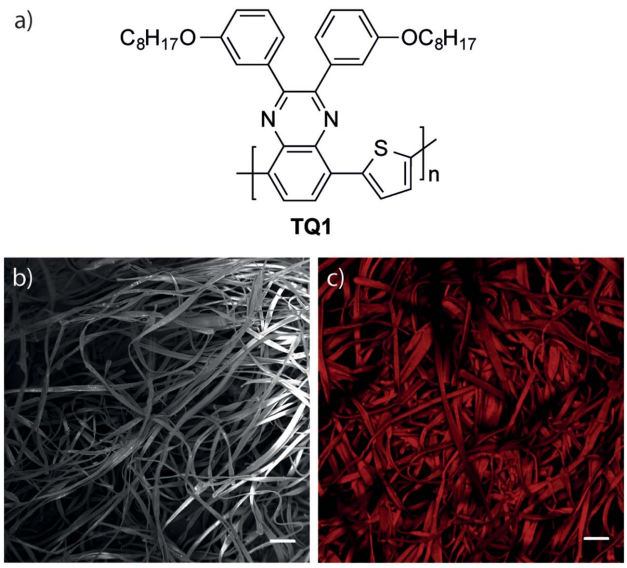

Figure 1. a) TQ1 molecular structure, b) scanning electron microscopy, and c) fluorescence microscopy images of electrospun TQ1. Scale bars: 50 μm.

2. Results and Discussion

2.1. Characterization of TQ1 Fibers

TQ1 (Figure 1a) was dissolved at a concentration of 12% (w/v) in chloroform and was electrospun using a traditional electrospinning setup and collected on aluminum foil. The electrospun TQ1 fibers were ribbon-like in structure with widths <10 μm (Figure 1b). This ribbon fiber morphology is similar to those seen when electrospinning collagen, gelatin, and silk,[26,27] and comparable to the structure of collagen fibrils found in, for example, the muscle of the heart.[28,29]

TQ1 is a low bandgap polymer that combines an electron rich donor moiety (thiophene) and an electron deficient acceptor moiety (quinoxaline).[23,30] The absorption spectra of spin-coated films of TQ1 show two distinct bands with peak maxima at 360 nm and approximately 620 nm, respectively (**Figure 2**). TQ1 was originally designed as a material for bulk heterojunctions in solar cells,[23] but quinoxaline-based compounds have also been extensively investigated for antitumor, antimicrobial, and antifungal properties.[31,32] Thiophenes, on the other hand, have been exhaustively used in the field of neural cell stimulation and regeneration,[33,34] and both quinoxaline and thiophene oligomers have been used as probes for amyloid plaques.[35–37] The aromatic heterocyclic structure of quinoxalines allow for intramolecular charge transfer, which renders the TQ1 polymer a low bandgap and highly fluorescent material. While most quinoxaline derivatives show an emission wavelength (λ_{em}) in the range between 430 and 607 nm,[14] when combined with the thiophene moiety in TQ1, the emission is broadly red shifted to around λ_{em} 720 nm (Figure 2).[38] Interestingly, the fluorescent properties of TQ1 are retained after electrospinning and the emission spectra of the fibers showed a similar emission profile as the film (Figure 2) but with a less pronounced shoulder region (760–820 nm).

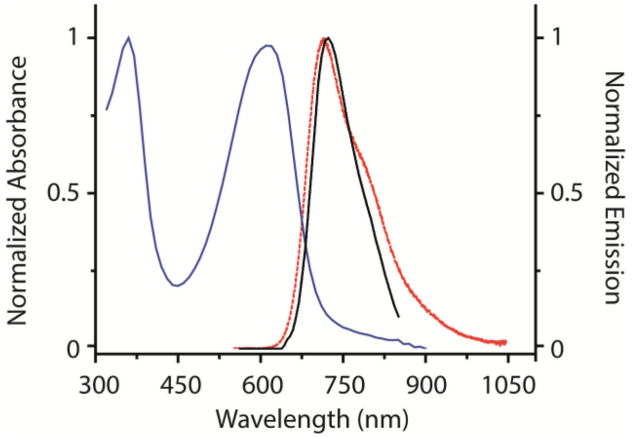

Figure 2. Normalized absorbance (blue, solid) and fluorescence emission spectra of TQ1 thin films excited at 533 nm (red, dashed). The absorbance spectrum shows maxima at 360 and 620 nm and the fluorescence emission appears at about 720 nm. Emission spectrum from a single TQ1 fiber (black, solid) obtained using wide-field spectral imaging show an emission maximum at about 730 nm.

The emission of the electrospun TQ1 is in the NIR region where the scattering and absorption coefficients of most tissues are at a minimum. NIR light can penetrate tissue up to several millimeters, and thus the TQ1 fibers have promising properties for in vivo tracking using noninvasive fluorescent imaging techniques.[39,40] In order to facilitate characterization of the material during in vitro and in vivo experiments, the electrospun TQ1 was physically adsorbed on the surface of polydimethylsiloxane (PDMS) and collagen hydrogels. The fibrous mats of TQ1 on PDMS (TQ1/PDMS) and collagen (TQ1/collagen) were similar in appearance with slight variations in surface coverage (**Figure 3**).

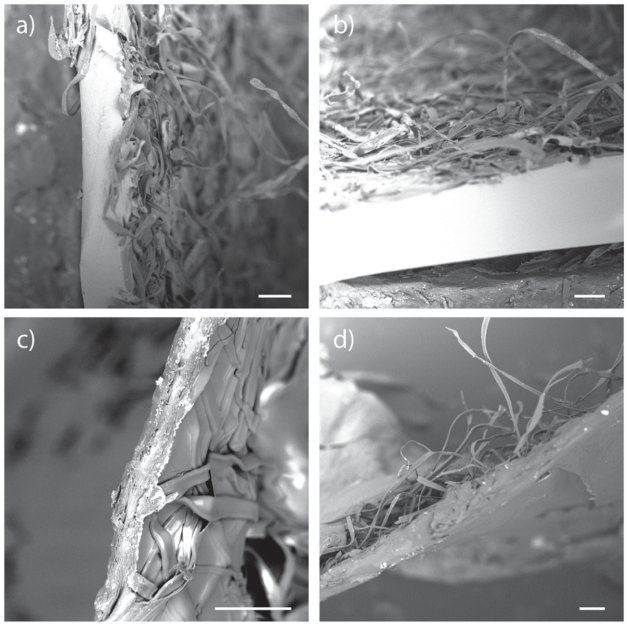

Figure 3. Scanning electron micrographs of electrospun TQ1 fibers physisorbed on a,b) PDMS and c,d) collagen hydrogel substrates. Scale bars: 50 μm.

The TQ1 fibers were transferred to the substrates by applying a piece of cured PDMS or by casting porcine collagen type I during crosslinking with *N*-hydroxysuccinimide (NHS) and 1-ethyl-3-(3-dimethylaminopropyl)carbodiimide (EDC) onto the electrospun material. Collagen hydrogels have been extensively used in various applications for tissue regeneration and is considered biocompatible and regeneration capable, and thus provides a suitable substrate for in vivo studies.[41,42] The cross-linked collagen hydrogels used here are very similar to materials that have been successfully used in humans in phase I clinical trials for cornea regeneration.[43] PDMS is also considered biocompatible but does not promote cell adhesion to the same extent as collagen and was utilized in order to better isolate the effect of the TQ1 fibers on cell adhesion and proliferation.[44,45]

The surface energy of a material has a great influence on the adsorption of proteins, considering protein adsorption is generally more prominent on hydrophobic low surface energy substrates.[46] Static contact angle measurements for water on TQ1 films and fibers, measured using the sessile drop technique, were 97° ± 4° and 133° ± 3°, respectively. Dispersive or Lifshitz–Van der Waals (γ^{LW}) surface free energy calculations of TQ1 films using the Good–van Oss–Chaudhury (GvOC) model[47] showed an overall surface energy of 29.2 mJ m^{-2} with negligible influences from polar components. The surface energy of TQ1 films was thus similar but slightly lower than that of the tissue culture plate (TCP) with and without fibronectin (38.9 ± 2.2 and 38.9 ± 0.7 mJ m^{-2}, respectively).[48] The water contact angle of fibronectin coated TCP, 97.6° ± 4.1°,[48] is similar to that of the TQ1 film. TCP/fibronectin are known to be the most favorable cell culture systems and the similarity in surface energy between TCP and TQ1 indicates that the latter also would promote cell adhesion. Adsorption of proteins from the cell culture medium was significant on TQ1 films as confirmed using staining with Coomassie blue (Figure S1a, Supporting Information). Due to difficulties with obtaining reliable data on contact angles for all solvents using the sessile drop technique on the TQ1 fibers, their surface energy could not be estimated. Previous investigations using an atomic force microscopy (AFM)-based technique comparing the surface energy of polyamide films and electrospun fibers with significantly smaller dimension (<250 nm) than the TQ1 fibers used here, however, showed that the fibers had about 20% higher surface free energy than films of the same material.[49] The significantly larger dimensions of the electrospun TQ1 fibers (3–10 μm) would, however, likely reduce any difference between the TQ1 fibers and films to a minimum.

2.2. Cell Viability and Proliferation on TQ1

In order to investigate the biocompatibility of the fibrous TQ1 scaffold, embryonic chicken cardiomyocytes (ECCM) cells and a mouse myoblast cell line (C2C12) were cultured on the TQ1 fibers using the different supporting substrates. Isolated ECCM cells cultured on the subtrates were characterized using a Live/Dead Viability/Cytotoxicity assay. At day 7 the cells were confluent on the tissue culture plate, collagen and TQ1/collagen

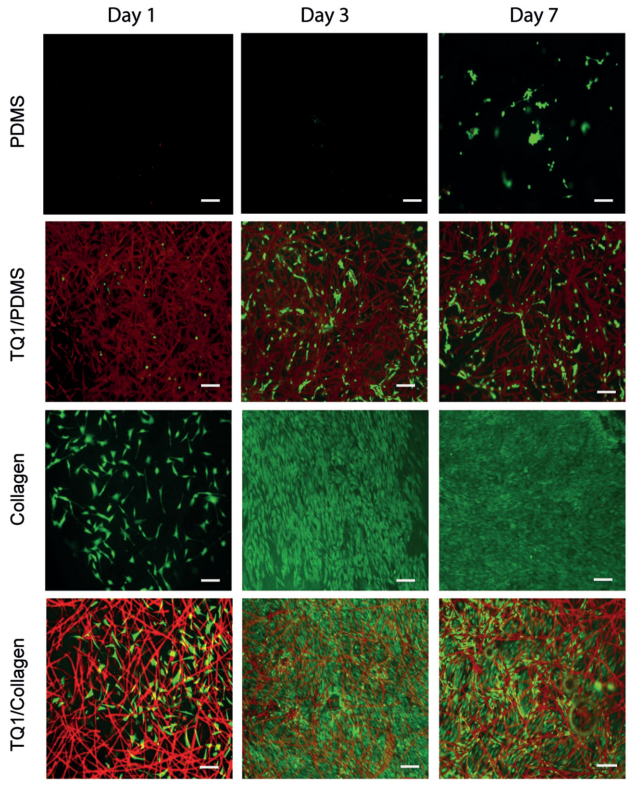

Figure 4. Cell viability of ECCM cells cultured on PDMS, TQ1/PDMS, collagen, and TQ1/collagen using the Live/Dead Viability/Cytotoxicity assay at days 1, 3 and 7. Scale bars: 50 μm.

samples (**Figure 4**). There was significant difference between the PDMS only and the TQ1/PDMS substrates, where the latter showed a higher number of viable cells. There was no evidence of cytotoxicity caused by the presence of the TQ1 fibers. When using PDMS as the supporting substrate, the ECCM cells showed preferential attachment on the TQ1 fibers rather than the substrate, which was clearly seen when using PDMS with a less dense fibrous mat of TQ1 (Figure S1b, Supporting Information).

Since there is a fluoresence overlap between the TQ1 and the red emission from dead cells from the ethidium homodimer-1 in the Live/Dead assay, ECCM cell proliferation was also investigated using a water soluble tetrazolium salt (WST-1) assay (Figure S2, Supporting Information). WST-1 is a spectrophotometric assay for characterization of proliferation and viability of cells that is not compromised by the presence of TQ1.

There was no significant difference ($p > 0.05$) between the the collagen substrate and the TQ1/collagen, but the presence of TQ1 on PDMS significantly increased cell proliferation as compared to PDMS alone ($p < 0$ .05) at day 7. Proliferation of C2C12 confirmed these results, demonstrating no significant difference between the collagen only substrate and the TQ1/collagen substrate at day 7 ($p > 0.05$) (Figure S3, Supporting Information). Materials that stimulate embryonic cardiomyocyte proliferation are important in the field of regenerative medicine, since these cells are vital in heart formation.[50,51] Likewise, C2C12 is a commonly used cell line that has implications in regeneration of smooth muscles and also in cardiac regeneration,[52,53] and the viability and proliferation of both these cell types on the TQ1 scaffold is very encouraging.

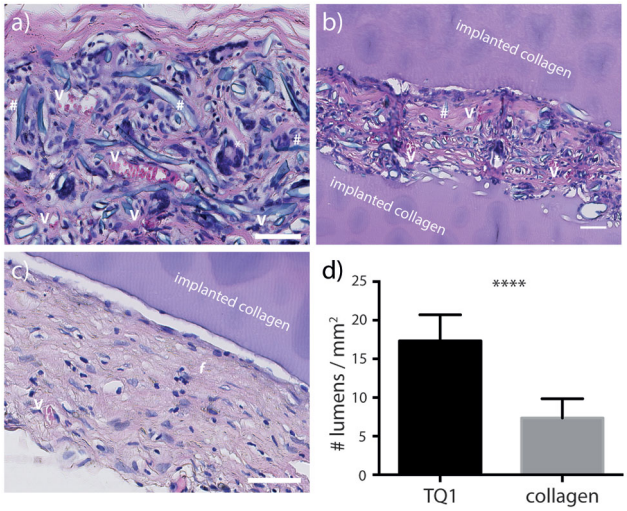

Figure 5. HE stained subcutaneous tissue sections from Wistar rats at 12 weeks with implants of a) TQ1, b) TQ1 sandwiched between collagen hydrogels, and c) collagen hydrogel. Fibrous tissue is indicated with *f* blood vessels with "V," "*" for multinucleated giant cells, and "#" for TQ1 (note: not all TQ1 fibers are marked). Scale bars: 50 μm. d) Number of lumens per mm^2 from implants with TQ1 and collagen hydrogel controls after three months.

2.3. Characterization of TQ1 in Tissue

Samples of electrospun TQ1 on collagen hydrogels were implanted subcutaneously into rats to evaluate the long-term cytotoxic or chronic inflammatory effects, and to investigate the possibility of tracking the material in the tissue using fluorescence imaging. No visible signs of inflammation were observed throughout the study. Histological evaluations using both standard hematoxylin and eosin (HE) staining and the intrinsic fluorescent properties of the TQ1 revealed striking differences between the TQ1 and the collagen sides of the implanted samples (**Figure 5** and Figure S4, Supporting Information). The TQ1 side, nearing the muscle of the rat, showed histiocytes, numerous lymphocytes, and the presence of multinucleated giant cells, where the TQ1 can be seen engulfed in its cytoplasm (Figure 5a and Figure S4d,f, Supporting Information). The HE staining also showed endogenous collagen integrated within the TQ1 fibers, and more importantly, numerous capillaries embedded in the fibrous TQ1 material (Figure 5a,b). Compared to the collagen controls the density of blood vessels was significantly higher for the TQ1 implants ($p < 0.0001$), Figure 5d. The apparent ability of the TQ1 scaffold to stimulate formation of blood vessels is of great interest for tissue regeneration,[54] but was unexpected as quinoxaline derivatives have previously been shown to inhibit vasculature endothelial growth factor (VGEF) stimulated angiogenesis.[55] The integration of the TQ1 fibers with the tissue was clearly seen using fluorescence microscopy imaging (**Figure 6**). The tissue formed

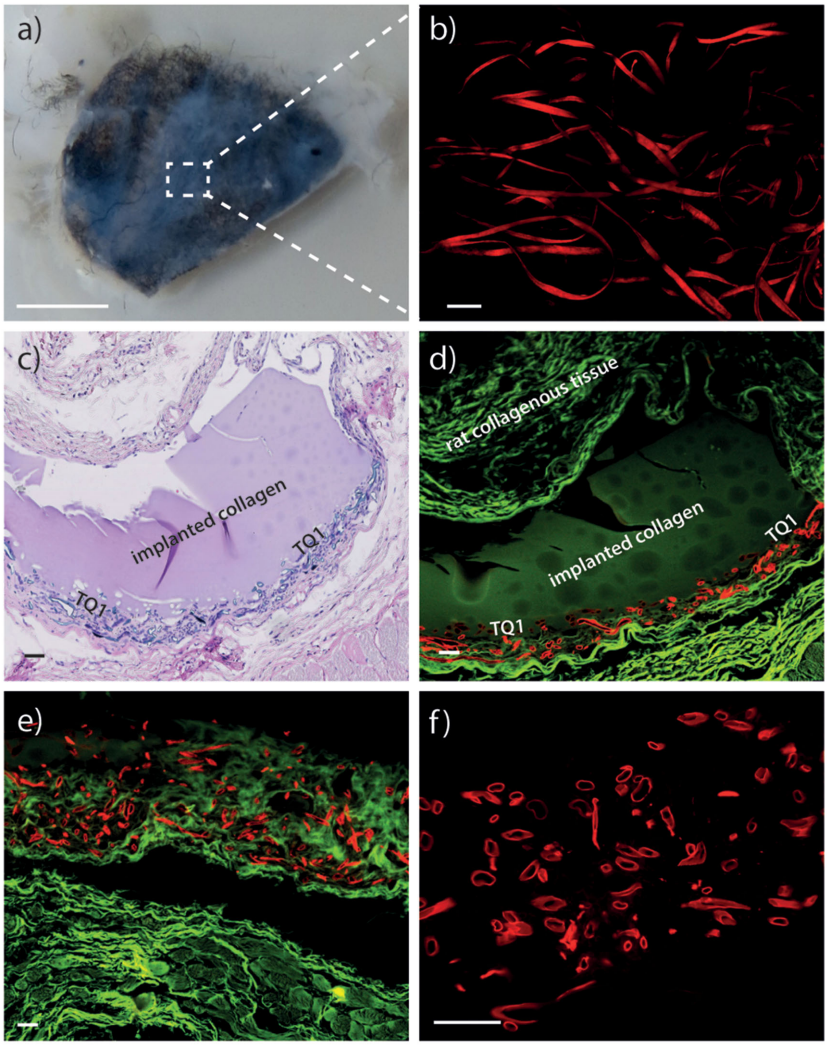

Figure 6. a) Resected TQ1 implant after 3 months in the subcutaneous tissue of the rat. Scale bar: 0.2 cm b) confocal fluorescence image of the TQ1 fibers within the full thickness implant. Scale bar: 50 μm. c) Light (HE stained), and d,e) fluorescence microscopy images of TQ1/collagen scaffolds implanted in subcutaneous tissue of Wistar rat. The HE stained endogenous and implanted collagen fluoresces at a lower wavelength (green) than the NIR emitting TQ1 when excited at 535 nm. f) TQ1 implants in tissue show no interference from tissue autofluorescence when excited at 640 nm. Scale bars: 50 μm.

completely around the TQ1 fibers, almost engulfing and removing them from the collagen substrates (Figure 6c). The collagen side and control samples, on the other hand, showed chronic inflammation, fewer blood vessels, and a pronounced fibrous capsule compared to the TQ1 side of the implant, (Figure 5c and Figure S4c,g–h, Supporting Information).

The TQ1 interaction in tissue not only showed diminished prolonged inflammation when compared to the collagen hydrogel interactions, but also full integration within the subcutaneous tissue. The fibrous capsule around the collagen, however, does not necessarily designate rejection, as this reaction is also commonly seen with other materials, including silk fibroin and collagen scaffolds.[56,57] Surface roughness is one variable that has a large influence on the inflammation responses and surfaces that are smooth on the macro and micro scale, like that of the collagen hydrogel used here, as it tends to elicit a response that stimulates fibrous capsule formation.[58,59] The different morphologies of the surfaces exposed to each tissue can also be a factor affecting chronic inflammation, which is more evident on the smoother collagen-tissue interface compared to the fibrous TQ1-tissue interface. No obvious degradation of the TQ1 fibers could be observed in the resected tissue after the three month implantation period.

The TQ1 fibers could be clearly distinguished in the resected tissue using confocal microscopy (Figure 6a,b). The autofluorescence of the surrounding tissue emits at a significantly lower wavelength than the TQ1, which facilitates tracking of the material (Figure S5c, Supporting Information). The wide-field spectral imaging in Figure S5 (Supporting Information) shows that the TQ1 fibers do not change their emission spectra when implanted. When excited at 640 nm the TQ1 scaffold can be imaged without interference from the surrounding tissue (Figure 6d) since the tissue autofluorescence is negligible in this wavelength range. The HE stained optical micrographs (Figure 6c and Figure S4, Supporting Information) and fluorescent images (Figure 6d,e) confirm the biocompatibility of the TQ1 and the ability to trace the fate and integration of the TQ1 fibers within the tissue.

Fluorescence lifetime imaging (FLIM) of TQ1 films showed a narrow distribution of fluorescence decays, around 100 ps, whereas electrospun TQ1 fibers and TQ1 fibers in tissue displayed a broader distribution of longer decays between 200 and 400 ps (**Figure 7**). The shorter decays as well as the defined shoulder in the fluorescence spectra of the TQ1 films indicate differences in molecular organization in the TQ1 film and the fibers. The polymer is known to form interchain aggregates as a result of π–π stacking in thin films.[23] The dimensions of the fibers are, however, significantly larger than the films used here (80 nm), which combined with the differences in processing for fiber and films, can result in large variations in polymer aggregation and organization. The color-coded fluorescence lifetime images show that the implantation of TQ1 fibers in tissue had little to no effect on the fluorescent decays from the fibers (Figure 7). The relatively short lifetime means that the molecule will be less vulnerable to excited state reactions (i.e., photobleaching, quenching, etc.), and will thus also be less phototoxic.[60] Additionally, the sub-nanosecond lifetimes of the TQ1 fibers are significantly shorter than the surrounding tissue, which significantly facilitates imaging and tracking of the material in the tissue (Figure 7c,d).

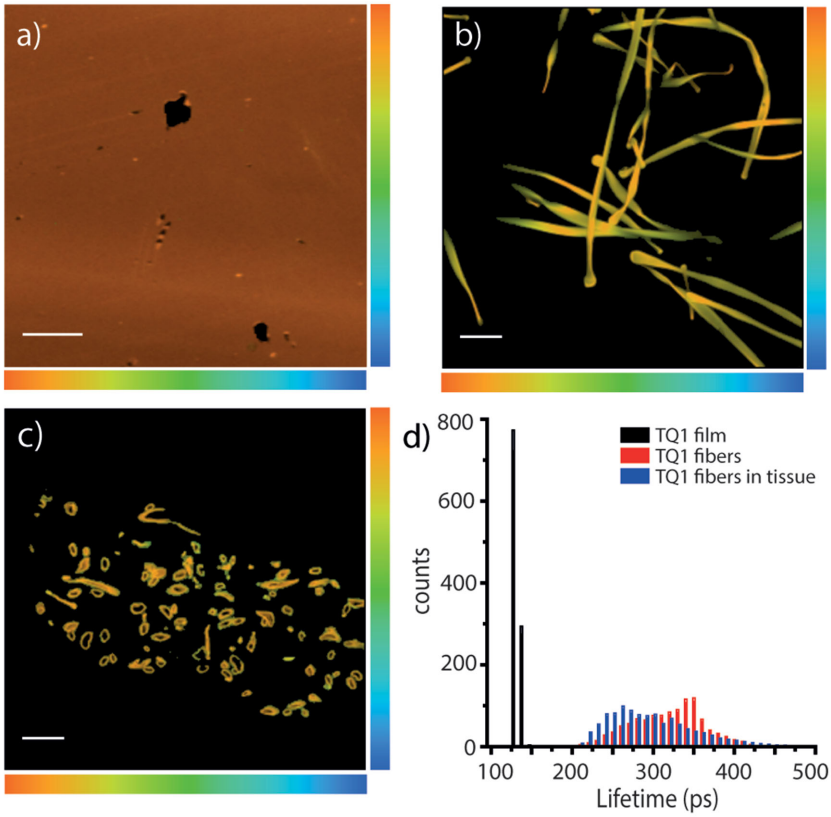

Figure 7. Fluorescent lifetime images a) a thin spun-coated film of TQ1 on a glass substrate, b) electrospun TQ1 fibers on a glass substrate and c) TQ1 fibers in tissue. Color bar denotes the fluorescent lifetimes from 100 ps (orange) to 1100 ps (blue). d) Histogram showing the distribution of fluorescence decays for TQ1 film (black), TQ1 fibers on glass (blue), and TQ1 fibers in tissue (red).

3. Conclusions

The rapid development of biofunctional polymer-based biomaterial scaffolds for tissue engineering is encouraging but suffers from difficulties with tracking the fate of implanted materials. We have successfully developed and thoroughly characterized a fibrous and biocompatible scaffold based on the luminescent low bandgap polymer TQ1. The TQ1 scaffold was prepared by electrospinning and the resulting fibers show a ribbon-like morphology with widths <10 µm. The TQ1 fibers emit in the NIR range and can be visualized in tissue using noninvasive fluorescence imaging and also demonstrate excellent biocompatibility, tissue integration, and stimulates formation of blood vessels within the implant. The tracking of the material in tissue is facilitated by the minimal overlap between the TQ1 and background and tissue autofluorescence emission spectra combined with the sub-nanosecond lifetimes of the TQ1 fibers. The latter also minimizes the phototoxicity of the material. The properties of the TQ1 scaffold make it an attractive biomaterial in its own right, but it can also be utilized to both improve the biocompatibility, angiogenic properties, and to enable convenient noninvasive tracking of other biomaterials.

4. Experimental Section

Chemicals: Chemicals were procured from Sigma-Aldrich, and used as received unless otherwise mentioned.

Material Fabrication: Poly[2,3-bis-(3-octyloxyphenyl)quinoxaline- 5,8-diyl-*alt*-thiophene-2,5-diyl] (TQ1), number-average molecular weight M_n = 24 kDa, weight average-molecular weight $\bar{M}_w$ = 65 kDa, and polydispersity index (PDI) = 2.7 was provided by Dr. Ergang Wang (Chalmers, Sweden). The synthesis of TQ1 is described in detail elsewhere.[23] TQ1 was dissolved at a concentration of 12% (w/v) in chloroform. Electrospinning was done with a traditional setup of the TQ1 solution in a 1 mL syringe connected to 20-gauge needle in an infusion pump (Chemyx Fusion 400, TX, USA). The solution was pumped out at a flow rate of 1 mL h^{-1} and subjected to 13.5 kV (Glassman High Voltage, NJ, USA) for 10 min. The fibers were collected on an aluminum foil attached to a grounded collector. The TQ1 was then physically immobilized onto polydimethylsiloxane, PDMS (Sylgard 186) 24 h after the PDMS had set at room temperature. Collagen/TQ1 samples were prepared by mixing 10% (w/v) porcine type I collagen (Sewon Cellontec Co., Seoul, South Korea) in a T-piece system with NHS and EDC.[42] The ratio of primary amines to EDC was calculated to 0.6 and EDC:NHS was kept at 1 M equivalent. The gel was casted onto the electrospun TQ1 mat and left between two glass slides with a 500 µm spacer overnight in a humidified container at room temperature. The gels were then transferred to an incubator for 5 h at 37 °C. TQ1 and control gels were then washed with 0.1 N sodium phosphate buffer before storing in 1X phosphate buffer saline (PBS) for further use.

Scanning Electron Microscopy (SEM): Samples were imaged immediately after fabrication using an FEI, Phenom Desktop SEM (Eindhoven, Netherlands) at an accelerating voltage of 5 kV. Collagen samples were first chemically dried using a series of 25%, 50%, and 70% alcohol washes for 5 min each, followed by 100% hexamethyldisilazane (HMDS) for 10 min. The samples were left under a fume hood before imaging.

Optical Characterizations: The TQ1 was dissolved in chloroform at a concentration of 0.6 wt% and a drop was applied on a glass substrate and spin-coated at 1000 rpm (Laurell Technologies, PA, USA). UV–vis spectra of the TQ1 films were recorded using a PerkinElmer Lambda 950 UV–vis Spectrophotometer (CA, USA). Photoluminescence was measured using an Oriel liquid light guide with a Shamrock SR 303i spectraphotograph attached to a Newton EMCCD silicon detector and excitation with a blue (405 nm) CW PMM-208G-VT laser pump (4 mW cm^{-2}) and green (532 nm) CW AGLM2 laser pump (5 mW cm^{-2}). Film thickness was calculated using the linear absorption maxima and thickness relationship for TQ1, to be approximately 80 nm.[61]

Confocal Imaging: The fluorescence emission spectral images were recorded with an inverted Zeiss (Axio Observer.Z1) LSM 780 microscope (Carl Zeiss MicroImaging GmbH, Jena, Germany) equipped with a 32 channel QUASAR GaAsP spectral array detector using a tunable In Tune laser (488–640 nm) (Carl Zeiss MicroImaging GmbH, Jena, Germany). Excitation utilized either the 488, 535, 565, or 625 nm laser output, using corresponding main beam splitters (f-MBS 488, f-MBS 405/535c, f-MBS 405/565c, or f-MBS 405/625c). For all acquisitions, the pinhole was set to 90 µm, scanning area was set to 42 427 × 42 427 µm, with a scanning resolution of 512 × 512 pixels. Further, a Plan-Apochromat 20×/0.8 objective lens was used.

Fluorescence Lifetime Imaging (FLIM): FLIM were acquired using an inverted Zeiss (Axio Observer.Z1) LSM 780 microscope (Carl Zeiss MicroImaging GmbH, Jena, Germany) equipped with a FLIM system from Becker & Hickl. Fluorescence emission was routed through the direct coupling (DC) confocal port of the Zeiss LSM 780 scanning unit and detected by a Becker & Hickl HPM-100–40 hybrid detector. Lifetime data were recorded by a Becker & Hickl Simple-Tau 152 system (SPC-150 TCSPC FLIM module) using the instrument recording software SPCM version 9.42 in the FIFO image mode, set at 256 × 256 pixels, using 256 time channels (Becker & Hickl GmbH, Berlin, Germany). Excitation utilized either the 535, 565, or 625 nm laser output from the tunable In Tune laser (Carl Zeiss MicroImaging GmbH, Jena, Germany) operating at 40 MHz, using corresponding main beam splitters (f-MBS 405/535c, f-MBS 405/565c, or f-MBS 405/625c). For all acquisitions, the pinhole was set to 20.2 µm, scanning area was set to 42 427 × 42 427 µm, with a scanning resolution of 512 × 512 pixels. Further, a Plan-Apochromat 20×/0.8 objective lens was used and a 510 nm longpass filter (510 ALP, XF3086 Omega Optical Inc., Brattleboro, Vermont, USA) was located in front of the hybrid PMT. Data were subsequently analyzed in SPCImage version 3.5.0.0 (Becker & Hickl GmbH, Berlin, Germany) fitting each of the acquired decay curves to a tri-exponential function. Histogram and color-coded images show the intensity-weighted average lifetime.

Wide-Field Spectral Imaging: Fluorescence images and spectra were recorded with a Leica DM6000 B fluorescence microscope (Leica Microsystems, Wetzlar, Germany) equipped with a HC PLAN APO 20×/0.7 PH2 objective lens (Leica Microsystems, Wetzlar, Germany), and filter cubes for 535 nm excitation ET535/50×, T565lprx, ET585lp [C-140878], or 640 nm excitation ET640/30×, T660LP, ET690/50m [C-140882](Chroma Technology Corporation, Bellows Falls, Vermont, USA). A Prior Lumen200 (Prior Scientific Ltd, Cambridge, UK) was utilized as light source and images were recorded with a SpectraCube spectral camera module with the acquisition software SpectraView (version 5.0.0.1) (Applied Spectral Imaging Ltd, Migdal Ha-Emek, Israel).

Surface Energy: Films of TQ1 were prepared by spin-coating a 12% (w/v) solution of TQ1 in chloroform onto a glass slide at 1000 rpm. Contact angle measurements were made using the sessile drop technique. The static and advancing angles of water, glycerol, and diiodomethane were obtained with a CAM 200 Optical Contact Angle Meter (KSV Instruments Ltd, Finland). The Gibbs surface energy was calculated using the GvOC model.[47]

In Vitro Cell Studies: All samples were kept in 1X penicillin/streptomycin in PBS until preparations for cell seeding. The samples were then incubated at 4 °C with 3X penicillin/streptomycin in PBS overnight and then washed 3X with sterile PBS just before cell seeding. Freshly isolated ECCM cells were a kind gift from Prof. Jordi Altimiras (Linköping University, Sweden). These cells were not used past passage 5. ECCM cells and C2C12 cells (obtained from Dr. L. Megeney, Ottawa Health Research Institute) were seeded on the materials at a density of 10^4 cells per well in a 96 well plate. Cells were maintained with DMEM supplemented with 10% Fetal Bovine Serum, 1% nonessential amino acids, and 1×10^{-3} M sodium pyruvate (Gibco, Life Technologies, CA, USA).

Proliferation Assay: WST-1 was done at day 1, 3, 5, and 7 for the C2C12, and day 1, 3, and 7 for the ECCM. 10 µL for C2C12 and 20 µL for ECCM of WST-1 (Roche, Life Technologies, CA, USA) was added to the samples and left to incubate for 0.5 h. 40 µL of media with WST-1 was then taken and placed into a different plate and the absorbance was read at 450 nm. An hour after first incubation, another 40 µL were taken and read to ensure that the OD numbers were saturated.

Live/Dead Assay: The Live/Dead assay was done in 96 wells plates for days 1, 3, and 7 for the ECCM using a Live/Dead Viability/Cytotoxicity Kit (Life Technologies, CA, USA) according to instructions provided by the manufacturer. The materials were imaged at each time point with a fluorescence microscope (Zeiss A 200M).

Subcutaneous Implantations in Rats: The study was approved by the ethics committee, Linköpings Djurförsöksetiska Nämnd, Linköping, Sweden and in compliance with the Swedish Animal Welfare Ordinance and the Animal Welfare Act. Four, 9 week old, Albino Wistar rats (Charles River, USA), weighting approximately 300 g each, were used for this study. All samples were stored in 1X penicillin/streptomycin in PBS and the day before the study the samples were trephine into 10 mm diameter circular grafts, washed twice in PBS and left overnight in 5X penicillin/streptomycin in PBS at 4 °C. The day of implantation, the rats were anaesthetized by inhalation of isoflurane (5% induction and 2% maintenance) through a nose cone inhaler. The rats were then shaven and the implantation site, the dorsum, was treated with 5% chlorhexidin and 70% alcohol. Paravertebral incisions were made 1 cm away from the vertebral column where the subcutaneous cavities were shaped on the left and right side of the upper and lower dorsum. One graft was placed on each side, the control and the sample, and then the incisions were secured with two to three interrupted sutures (5.0 absorbable Vicryl). The rats were maintained for 90 d and a licensed veterinarian monitored the rats for healing, skin appearance, and re-growth of hair after surgery.

Histological Evaluations: The rats were anaesthetized with isoflourane then the dorsal area was shaved and the implants were removed along with surrounding tissues. The rats were then euthanized with pentobarbital. The samples were fixed in 4% formaldehyde and 0.1 M phosphate buffered saline for 4 d then were fixed in paraffin. For histology, 5–8 µm slices were cut (Leica RM2235) and then stained with hematoxylin (Harris Histolab, Sweden) and eosin. The slides were evaluated using an Olympus BX50 microscope.

Statistical Analysis: Statistical analysis on WST-1 curves was carried using either student *t*-test or ANOVA with GraphPad Prism (La Jolla CA, USA). Statistical significance was assigned at a value of $p < 0.05$ and are indicated with an asterisk, (*). p values > 0.05 were denoted as not significant and labeled as "ns."

Supporting Information

Supporting Information is available from the Wiley Online Library or from the author.

Acknowledgements

Thanks to Prof. Torkel Erhardsson for statistical guidance, to Jonas Bergqvist for help with photoluminescent data acquisition, Anders Elfwing, Dr. Luigi Petrone, Dr. Koen Vandewal, Dr. Naresh Polsetti, Prof. Klas I. Udekwu, and Prof. Olle Inganäs for help with initial experiments. Also, thanks to Dr. Staffan Dånmark for reviewing the manuscript. Prof. Jordi Altimiras kindly provided the ECCM (Linköping University, Sweden). D.A. and A.W. gratefully acknowledge financial support from Linköping University and the Swedish Foundation for Strategic Research. K.P.R.N. and D.S. acknowledge the support by the Swedish Foundation for Strategic Research. E.W. thanks the Swedish Research Council for financial support. During this study, A.W. was enrolled in the graduate school Forum Scientium.

Received: January 27, 2015
Revised: April 15, 2015
Published online: May 28, 2015

[1] J. D. Kretlow, A. G. Mikos, *AIChE J.* **2008**, *54*, 3048.
[2] J. Hilborn, L. M. Bjursten, *J. Tissue Eng. Regen. Med.* **2007**, *1*, 110.
[3] R. E. J. Akins, D. Rockwood, K. G. Robinson, D. Sandusky, J. Rabolt, C. Pizarro, *Tissue Eng., Part A* **2010**, *16*, 629.
[4] W. J. Li, R. Tuli, X. Huang, P. Laquerriere, R. S. Tuan, *Biomaterials* **2005**, *26*, 5158.
[5] R. D. Breukers, K. J. Gilmore, M. Kita, K. K. Wagner, M. J. Higgins, S. E. Moulton, G. M. Clark, D. L. Officer, R. M. I. Kapsa, G. G. Wallace, *J. Biomed. Mater. Res.* **2010**, *95A*, 256.

[6] E. C. Novosel, C. Kleinhans, P. J. Kluger, *Adv. Drug Delivery Rev.* **2011**, *63*, 300.
[7] S. Fuchs, S. Ghanaati, C. Orth, M. Barbeck, M. Kolbe, A. Hofmann, M. Eblenkamp, M. Gomes, R. L. Reis, C. J. Kirkpatrick, *Biomaterials* **2009**, *30*, 526.
[8] L. Heinrich, A. M. Freyria, M. Melin, Y. Tourneur, R. Maksoud, J. C. Bernengo, D. J. Hartmann, *J. Biomed. Mater. Res., Part B* **2006**, *81B*, 153.
[9] S. H. Kim, G. Park, H. Hyun, J. H. Lee, Y. Ashitate, J. Choi, G. H. Hong, E. A. Owens, M. Henary, H. S. Choi, *Biomed. Mater.* **2013**, *8*, 014110.
[10] E. Bible, F. Dell'Acqua, B. Solanky, A. Balducci, P. M. Crapo, S. F. Badylak, E. T. Ahrens, M. Modo, *Biomaterials* **2012**, *33*, 2858.
[11] A. C. Jones, B. Milthorpe, H. Averdunk, A. Limaye, T. J. Senden, A. Sakellariou, A. P. Sheppard, R. M. Sok, M. A. Knackstedt, A. Brandwood, D. Rohner, D. W. Hutmacher, *Biomaterials* **2004**, *25*, 4947.
[12] A. A. Appel, M. A. Anastasio, J. C. Larson, E. M. Brey, *Biomaterials* **2021**, *34*, 6615.
[13] M. Z. Lin, M. R. McKeown, H.-L. Ng, T. A. Aguilera, N. C. Shaner, R. E. Campbell, S. R. Adams, L. A. Gross, W. Ma, T. Alber, R. Y. Tsien, *Chem. Biol.* **2009**, *16*, 1169.
[14] S. Achelle, C. Baudequin, N. Plé, *Dyes Pigm.* **2021**, *98*, 575.
[15] A. M. Smith, M. C. Mancini, S. Nie, *Nat. Nanotechnol.* **2009**, *4*, 710.
[16] N. Fomina, C. McFearin, M. Sermsakdi, O. Edigin, A. Almutairi, *J. Am. Chem. Soc.* **2010**, *132*, 9540.
[17] A. D. Bendrea, L. Cianga, I. Cianga, *J. Biomater. Appl.* **2011**, *26*, 3.
[18] A. Laforgue, L. Robitaille, *Macromolecules* **2010**, *43*, 4194.
[19] R. Balint, N. J. Cassidy, S. H. Cartmell, *Acta Biomater.* **2014**, *10*, 2341.
[20] B. M. Wegenast-Braun, A. Skodras, G. Bayraktar, J. Mahler, S. K. Fritschi, T. Klingstedt, J. J. Mason, P. Hammarström, K. P. R. Nilsson, C. Liebig, M. Jucker, *Am. J. Pathol.* **2012**, *181*, 1953.
[21] D. Ding, K. Li, Z. Zhu, K.-Y. Pu, Y. Hu, X. Jiang, B. Liu, *Nanoscale* **2011**, *3*, 1997.
[22] Y. Yuan, D. Ding, K. Li, J. Liu, B. Liu, *Small* **2014**, *10*, 1967.
[23] E. Wang, L. Hou, Z. Wang, S. Hellström, F. Zhang, O. Inganäs, M. R. Andersson, *Adv. Mater.* **2010**, *22*, 5240.
[24] V. Ntziachristos, *Nat. Methods* **2010**, *7*, 603.
[25] A. Nwaneshiudu, C. Kuschal, F. H. Sakamoto, R. R. Anderson, K. Schwarzenberger, R. C. Young, *J. Invest. Dermatol.* **2012**, *132*, e3.
[26] M. Li, M. J. Mondrinos, M. R. Gandhi, F. K. Ko, A. S. Weiss, P. I. Lelkes, *Biomaterials* **2005**, *26*, 5999.
[27] X. Zhang, M. R. Reagan, D. L. Kaplan, *Adv. Drug Delivery Rev.* **2009**, *61*, 988.
[28] J. R. Harris, A. Reiber, *Micron* **2006**, *38*, 513.
[29] M. Eghbali, K. T. Weber, *Mol. Cell. Biochem.* **1989**, *96*, 1.
[30] S. Hedström, P. Persson, *J. Phys. Chem. C* **2012**, *116*, 26700.
[31] T. Biswas, O. E. Zolova, F. Lombó, F. de la Calle, J. A. Salas, O. V. Tsodikov, S. Garneau-Tsodikova, *J. Mol. Biol.* **2010**, *397*, 495.
[32] K. Toshima, R. Takano, T. Ozawa, S. Matsumura, *Chem. Commun.* **2002**, *3*, 212.
[33] P. Fattahi, G. Yang, G. Kim, M. R. Abidian, *Adv. Mater.* **2014**, *26*, 1846.
[34] R. A. Green, N. H. Lovell, G. G. Wallace, L. A. Poole-Warren, *Biomaterials* **2008**, *29*, 3393.
[35] M. Cui, M. Ono, H. Kimura, B. Liu, H. Saji, *Bioorg. Med. Chem. Lett.* **2011**, *21*, 4193.
[36] A. Åslund, C. J. Sigurdson, T. Klingstedt, S. Grathwohl, T. Bolmont, D. L. Dickstein, E. Glimsdal, S. Prokop, M. Lindgren, P. Konradsson, D. M. Holtzman, P. R. Hof, F. L. Heppner, S. Gandy, M. Jucker, A. Aguzzi, P. Hammarström, K. P. R. Nilsson, *ACS Chem. Biol.* **2009**, *4*, 673.
[37] K. Arja, D. Sjölander, A. Åslund, S. Prokop, F. L. Heppner, P. Konradsson, M. Lindgren, P. Hammarström, K. O. A. Åslund, K. P. R. Nilsson, *Macromol. Rapid Commun.* **2013**, *34*, 723.
[38] L. Hou, E. Wang, J. Bergqvist, B. V. Andersson, Z. Wang, C. Müller, M. Campoy-Quiles, M. R. Andersson, F. Zhang, O. Inganäs, *Adv. Funct. Mater.* **2011**, *21*, 3169.
[39] J. Frangioni, *Curr. Opin Chem. Biol.* **2003**, *7*, 626.
[40] S. Selvam, K. Kundu, K. L. Templeman, N. Murthy, A. J. García, *Biomaterials* **2011**, *32*, 7785.
[41] W. Friess, *Eur. J. Pharm. Biopharm.* **1997**, *45*, 113.
[42] Y. Liu, M. Griffith, M. A. Watsky, J. V. Forrester, L. Kuffová, D. Grant, K. Merrett, D. J. Carlsson, *Biomacromolecules* **2006**, *7*, 1819.
[43] P. Fagerholm, N. S. Lagali, K. Merrett, W. B. Jackson, R. Munger, Y. Liu, J. W. Polarek, M. Soderqvist, M. Griffith, *Sci. Transl. Med.* **2010**, *2*, 46r61.
[44] G. M. Whitesides, *Nature* **2006**, *442*, 368.
[45] N. D. Evans, C. Minelli, E. Gentleman, V. LaPointe, S. N. Patankar, M. Kallivretaki, X. Chen, C. J. Roberts, M. M. Stevens, *Eur. Cells Mater.* **2009**, *18*, 1.
[46] E. Ostuni, B. A. Grzybowski, M. Mrksich, C. S. Roberts, G. M. Whitesides, *Langmuir* **2003**, *19*, 1861.
[47] L. Petrone, A. Di Fino, N. Aldred, P. Sukkaew, T. Ederth, A. S. Clare, B. Liedberg, *Biofouling* **2011**, *27*, 1043.
[48] E. M. Harnett, J. Alderman, T. Wood, *Colloids Surf. B* **2007**, *55*, 90.
[49] U. Stachewicz, A. H. Barber, *Langmuir* **2011**, *27*, 3024.
[50] J. Xie, Q. Zhang, T. Zhu, Y. Zhang, B. Liu, J. Xu, H. Zhao, *Acta Biomater.* **2014**, *10*, 2463.
[51] C. Bai, L. Hou, M. Zhang, L. Wang, W. Guan, Y. Ma, *Cell Prolif.* **2013**, *46*, 232.
[52] S. Burattini, P. Ferri, M. Battistelli, R. Curci, F. Luchetti, E. Falcieri, *Eur. J. Histochem.* **2011**, *48*, 223.
[53] L. Formigli, F. Francini, R. Squecco, D. Nosi, L. Polidori, S. Nistri, L. Chiappini, V. Cesati, A. Pacini, A. M. Pern, G. E. Orlandini, S. Z. Orlandini, D. Bani, *Am. J Physiol: Cell Physiol.* **2004**, *288*, C795.
[54] E. S. Place, N. D. Evans, M. M. Stevens, *Nature* **2009**, *8*, 457.
[55] J. L. Whatmore, E. Swann, P. Barraja, J. J. Newsome, M. Bunderson, H. D. Beall, J. E. Tooke, C. J. Moody, *Angiogenesis* **2002**, *5*, 45.
[56] Y. Shen, S. L. Redmond, J. M. Papadimitriou, B. M. Teh, S. Yan, Y. Wang, M. D. Atlas, R. J. Marano, M. Zheng, R. J. Dilley, *Biomed. Mater.* **2014**, *9*, 1.
[57] C. Fredriksson, M. Hedhammar, R. Feinstein, K. Nordling, G. Kratz, J. Johansson, F. Huss, A. Rising, *Materials* **2009**, *2*, 1908.
[58] M. A. Laflamme, C. E. Murry, *Nature* **2011**, *473*, 326.
[59] D. F. Williams, *Biomaterials* **2008**, *29*, 2941.
[60] R. A. Hoebe, C. H. Van Oven, T. W. J. Gadella, P. B. Dhonukshe, C. J. F. Van Noorden, E. M. M. Manders, *Nat. Biotechnol.* **2007**, *25*, 249.
[61] T. Tromholt, M. V. Madsen, J. E. Carlé, M. Helgesen, F. C. Krebs, *J. Mater. Chem.* **2012**, *22*, 7592.